Iranian Journal of Pharmaceutical Sciences
2026: 22 (1): 124-134
https://journals.sbmu.ac.ir/IJPS

Research Article

OPEN ACCESS

Phytochemical Characterization and Skin Cancer Inhibitory Potential of *Ficus hispida* Methanolic Extract: Insights from Molecular Docking and Cell-Based Assays

Murali Prakash Jatla [a], Deepti Kolli[a]*

[a] *Department of Chemistry, Koneru Lakshmaiah Education Foundation, Greenfields, Vaddeswaram, Guntur-522302, Andhra Pradesh, India.*

Received: May 27, 2025 **Last Revision:** October 20, 2025 **Accepted:** November 5, 2025 **Available online:** April 08, 2026.

Abstract

This study investigates the anticancer potential of *Ficus hispida* fruit extract, focusing on its phytochemical composition and molecular interactions with skin cancer targets. Fruits were collected from Jamia Salafiya Pharmacy College, and 500 g were subjected to Soxhlet extraction using methanol, yielding a concentrated ethyl acetate extract. LC-MS/MS analysis identified key bioactive compounds, including quercetin (m/z 302.33), kaempferol (m/z 284.26), gallic acid (m/z 169.14), lupeol (m/z 434.48), and β-sitosterol (m/z 414.58), confirming the extract's chemical diversity. In-silico molecular docking showed that gallic acid exhibited notable binding affinities with skin cancer-related proteins: 1M17 (-6.3 kcal/mol), 4QTB (-5.4 kcal/mol), and 5MP8 (-5.6 kcal/mol). Hydrogen bonding, van der Waals interactions, and π-alkyl interactions were observed, particularly with residues Asp831, Arg-84, and Asn118, indicating the formation of stable ligand-protein complexes. Molecular dynamics (MD) simulations further validated stability, with low RMSD (2.0 Å) and compact radius of gyration (19.8 Å). MM-GBSA binding free energy analysis yielded a favorableΔG_bind of -58.61 kcal/mol for the gallic acid-1P7K complex. *In vitro* MTT assays revealed dose-dependent cytotoxicity of gallic acid against SKML skin cancer cells, with an IC50 value of 13.601±0.488 µg/mL. AO/EB staining confirmed effective induction of apoptosis in treated cells. These results collectively highlight the effectiveness of gallic acid from *Ficus hispida* as a promising candidate for skin cancer therapy, warranting further preclinical and clinical investigations for therapeutic development.

Keywords: *Ficus hispida*; Gallic acid; Skin cancer; Molecular docking; Phytochemical analysis.

1. Introduction

Skin cancer is the most prevalent form of cancer globally, arising from the uncontrolled growth of abnormal skin cells [1]. It primarily develops in areas exposed to ultraviolet (UV) radiation, such as the face, neck, and arms, but can occur anywhere on the body [2]. The three main types of skin cancer are basal cell carcinoma (BCC), squamous cell carcinoma (SCC), and melanoma. BCC and SCC, collectively known as nonmelanoma skin cancers, are more common and generally less aggressive. Melanoma, though less frequent, is highly malignant and responsible for the majority of skin cancer-related deaths due to its propensity for rapid metastasis [3]. The incidence of skin

*** Corresponding Author**:
Deepti Kolli, Department of Chemistry, Koneru Lakshmaiah Education Foundation, Greenfields, Vaddeswaram, Guntur-522302, Andhra Pradesh, India. E-mail: atluri.deepti1984@gmail.com.

Cite this article as: Jatla M.P. Kolli D. Phytochemical Characterization and Skin Cancer Inhibitory Potential of *Ficus hispida* Methanolic Extract: Insights from Molecular Docking and Cell-Based Assays. Iran. J. Pharm. Sci., 2026, 22 (1): 124-134.

DOI: https://doi.org/10.22037/ijps.v22i1.48525

cancer has been rising steadily, attributed to factors such as increased UV exposure, fair skin phenotype, genetic predisposition, immunosuppression, and environmental influences [1, 3]. Early detection is crucial, as prognosis and survival rates are significantly higher when the disease is identified at an initial stage. However, many cases are diagnosed late, especially in populations with limited access to healthcare or awareness, leading to more advanced disease and poorer outcomes [4]. Treating skin cancer presents several challenges and complications, depending on the type, stage, and location of the tumor. Surgical excision remains the gold standard for localized nonmelanoma skin cancers, offering high cure rates. However, surgery can be complicated by tumor size, depth, and proximity to critical anatomical structures, sometimes resulting in disfigurement, functional impairment, or incomplete removal. In cases of advanced or metastatic disease, surgery may not be feasible, necessitating the use of radiotherapy, chemotherapy, or targeted therapies [4].

Phytomedicine, the use of plant-derived compounds for therapeutic purposes, has gained considerable attention in recent years as a promising alternative or complement to conventional cancer treatments [5]. The rich chemical diversity found in medicinal plants offers a vast reservoir of bioactive molecules with unique mechanisms of action, many of which remain untapped by modern medicine. In the context of skin cancer, phytomedicine holds particular importance due to its potential to provide safer, more affordable, and less toxic therapeutic options compared to traditional chemotherapeutic agents, which often cause significant side effects and face challenges such as drug resistance [6].

Ficus hispida, commonly known as the hairy fig, has emerged as a valuable medicinal plant with significant promise in cancer therapy, particularly for skin cancer [7]. Traditionally used in various Asian healing systems, its fruits are rich in a diverse array of bioactive phytochemicals, as revealed by advanced LC-MS/MS analysis. Key constituents such as gallic acid [8], quercetin [9], kaempferol [10], lupeol [11], and β-sitosterol [12] have been identified in the methanolic extract, each known for potent antioxidant, anti-inflammatory, and anticancer properties. The present study identifies the bioactive compounds in the methanolic extract of Ficus hispida and investigates their in-silico and in vitro skin cancer activity.

2. Materials and Methods

2.1. Ficus hispida fruit collection and identification

A plant sample was gathered from Vaddeswaram, Andhra Pradesh, India (16.441554°N, 80.615216°E), with the exact location and collection time (May 22, 2025, 1:26 PM IST) recorded using a GPS-enabled camera. Only healthy, mature leaves and stems were chosen to ensure the sample's quality for subsequent analysis. The collection process was overseen by Dr. K. Deepti from the Department of Chemistry at K L University, Guntur District. Dr. P. Satyanarayana Raju, a taxonomist from the Department of Botany and Microbiology at Acharya Nagarjuna University, identified the specimen. A detailed examination of morphological features, including leaf shape, arrangement, venation, and stem characteristics, was carried out. These observations were compared with established taxonomic references and herbarium specimens, confirming the plant as *Ficus hispida* L.f., a member of the Moraceae family.

2.2. Extraction Hot Continuous Extraction-Soxhlet

500 g of shade-dried *Ficus hispida* fruits were ground and placed in a filter paper thimble, which was loaded into chamber E of a Soxhlet apparatus. Methanol, chosen for its efficiency in dissolving a wide range of phytochemicals, was heated in flask A, vaporised, and condensed in condenser D before dripping onto the plant material. The extraction process relied on continuous solvent recycling, facilitated by a siphon mechanism that transferred liquid back to flask A once the chamber reached a specific level. This cyclic process thoroughly extracted bioactive compounds from the plant material. The procedure continued until a drop of solvent from the siphon tube evaporated without residue, indicating completion. The resulting crude ethyl acetate extract, saturated with bioactive compounds, was carefully preserved for subsequent phytochemical analysis [13, 14].

2.3. Phytochemical analysis by using LC-MS analysis

The methanolic extract underwent molecular weight analysis using an LC-MS/MS system (Shimadzu 8045). The extract was diluted to 10 µL, vortexed immediately, and centrifuged at 10,000 rpm for 10 minutes. The

supernatant was filtered through Whatman Grade 41 filter paper, and the filtrate was stored at 18°C for phytochemical studies. The mobile phases comprised 0.5% acetic acid (v/v) and pure methanol. An isocratic elution protocol was employed, consisting of 55% acetic acid (0–10 min), 65% (11–20 min), and 35% (21–30 min). The PDA detector (HPLC, 340 nm wavelength) operated with a column temperature of 30°C. The mass spectrometer used a positive ionization mode, scanning from 150 to 1000 m/z, with a capillary voltage of 3.50 kV, a cone voltage of 30 V, an extractor voltage of 3 V, a gas flow of 30 L/h, and a collision gas flow of 0.18 mL/min [15].

2.4. In-silico skin cancer activity of the phytochemicals

To comprehensively explore the binding interactions between the major skin cancer target proteins 1M17, 4QTB, and 5MP8 and the ligands like Quercetin, Kaempferol, Gallic acid, Lupeol, β-sitosterol, Psoralen, and Bergapten, molecular docking simulations were conducted using AutoDock 4.2.6 [16].

The proteins 1M17, 4QTB, and 5MP8 were carefully selected for molecular docking studies due to their key roles in cancer-related signaling pathways. 1M17 corresponds to the kinase domain of the human Epidermal Growth Factor Receptor (EGFR). This receptor tyrosine kinase is often overexpressed in numerous cancers and is an established target for anticancer therapeutics. 4QTB represents human Mitogen-Activated Protein Kinase 3 (MAPK3/ERK1), a central component of the MAPK/ERK pathway, which transduces mitogenic and stress signals crucial for cell proliferation and survival, and is frequently dysregulated in oncogenesis. 5MP8, though less characterized structurally, refers to a protein involved in translational regulation and cancer, with emerging evidence indicating its role in modulating non-canonical translation initiation, thereby impacting oncogenic protein synthesis. Docking these proteins with lead phytochemicals enables detailed analyses of binding interactions, supporting the rationale for targeted anticancer strategies.

Prior to docking, the three-dimensional structures of both the receptor proteins and the ligand were meticulously prepared by converting them into the pdbqt format, ensuring the proper addition of non-polar hydrogens to optimize molecular flexibility and accuracy in interaction predictions [17]. The docking simulations were configured with precise parameters to achieve reliable and reproducible results. A grid box was defined around the active binding site of each protein, carefully calibrated with specific dimensions to encompass the ligand's potential binding regions while maintaining a grid spacing of 0.3 Å to balance computational efficiency and resolution [18]. The docking process was executed using the Lamarckian Genetic Algorithm (LGA), a widely adopted optimization method that enhances conformational sampling by incorporating evolutionary principles and local search refinement [19]. Each molecular docking experiment consisted of three independent runs to ensure statistical robustness and minimize variability in binding predictions. For each run, 50 docking solutions were generated, with a population size of 500 individuals, 2,500,000 energy evaluations, and a maximum of 27 generations. Default settings were maintained for all other parameters to preserve the integrity of the docking protocol. The docking simulations aimed to identify the most favourable binding conformations of phytochemicals within the active sites of the target proteins, providing insights into potential molecular interactions and binding affinities that could inform further experimental validation and drug design studies.

2.5. Molecular Dynamics Simulation

Molecular dynamics (MD) simulations were carried out using Desmond 2020.1 on the top-ranked protein-ligand complex with gallic acid. The system was prepared with the OPLS-2005 force field and solvated using an explicit SPC water model within a cubic periodic boundary box measuring 1.0 Å on each side [20, 21]. To ensure charge neutrality, sodium ions (Na^+) were added, and a 0.15 M NaCl solution was included to mimic physiological conditions [22]. The simulation protocol began with a 10-nanosecond equilibration under an NVT ensemble, followed by a 12-nanosecond NPT equilibration and minimization phase using the Nose-Hoover chain coupling method, maintaining a relaxation time of 1.0 picoseconds and a pressure of 1 bar. The main production run was conducted for 100 nanoseconds with a 2-

femtosecond time step, utilizing the RESPA integrator for bonded interactions. Long-range electrostatic interactions were handled using the particle mesh Ewald method with a 9 Å cutoff, and pressure was regulated with the Martyna-Tuckerman-Klein barostat set to a 2-picosecond relaxation period. Throughout the simulations, temperature was controlled with a constant relaxation time of 1.0 picoseconds. To evaluate the stability of the MD simulations, key parameters, including root mean square deviation (RMSD), radius of gyration (Rg), root mean square fluctuation (RMSF), and the number of hydrogen bonds, were analyzed [23].

2.6. Binding free energy analysis

The binding free energies of ligand-protein complexes were estimated using the Molecular Mechanics/Generalized Born Surface Area (MM-GBSA) method. This analysis was performed using the thermal_mmgbsa.py Python script, which applied the OPLS5 force field and the VSGB solvation model to the last 50 frames of the simulation trajectory, sampled at every frame. The MM-GBSA approach calculates binding energy by summing various energy components, including electrostatic (Coulombic), covalent, hydrogen bonding, van der Waals, self-contact, lipophilic, and solvation energies for both the ligand and the protein. These individual contributions are combined according to the principle of additivity to yield the total binding free energy [24]. The equation used to calculate ΔG_{bind} is the following:

$$\Delta G_{bind} = \Delta G_{MM} + \Delta G_{Solv} - \Delta G_{SA}$$

Where

- **ΔG_{bind}** represents the free energy change associated with ligand binding,
- **ΔG_{MM}** refers to the variation in molecular mechanics energies between the ligand-protein complex and the individual, unbound forms of the ligand and protein.
- **ΔG_{Solv}** denotes the change in solvation free energy, calculated as the difference between the solvation energy of the ligand-receptor complex and the combined solvation energies of the free ligand and receptor.
- **ΔG_{SA}** accounts for the change in surface area-related energy between the bound and unbound states of the protein and ligand.

2.7. In-vitro skin cancer activity of the gallic acid

SKML cell viability was assessed using an MTT assay. Viable cells were first counted with a hemocytometer, then diluted in DMEM to a concentration of 1×10^4 cells/ml and seeded into 96-well plates, allowing them to adhere for 24 hours. After attachment, cells were exposed to varying concentrations of the test samples (10–50 µg/mL) and incubated for an additional 24 hours at 37°C in an atmosphere containing 5% CO_2 and 95% air. Following treatment, the wells were washed with fresh medium, and MTT solution (5 mg/ml in PBS) was added. The plates were then incubated for an additional 4 hours at 37°C to allow for the formation of formazan. The resulting purple formazan crystals were dissolved in 100 µl of DMSO per well, and absorbance was measured at 540 nm using a microplate reader. Cell viability was calculated as a percentage relative to untreated control cells, and IC_{50} values were determined from the data [25, 26].

$$\text{Inhibitory of cell proliferation (\%)} = \frac{\text{Mean absorbence of the control} - \text{Mean absorbence of the sample}}{\text{Mean absorbence of the control}} \text{ X } 100$$

2.8. Measurement of apoptotic induction using the acridine orange/ethidium bromide (AO/EB) dual staining method

SKML cells were plated at a density of 5 × 10^4 cells per well in 6-well plates and incubated for 24 hours. Following exposure to Sample 147 at a concentration of 40 µg/mL for an additional 24 hours, the cells were detached and rinsed with cold phosphate-buffered saline (PBS). The cells were then stained at room temperature for 5 minutes using a 1:1 mixture of acridine orange (AO) and ethidium bromide (EB), each at a concentration of 100 µg/ml. After staining, the cells were immediately examined under a fluorescence microscope at 20x magnification to assess morphological changes [27, 28].

3. Results and Discussion

3.1. Phytochemical analysis by using LC-MS analysis

LC-MS analysis of the *Ficus hispida* ethyl acetate extract identified key phytochemicals across multiple classes, with flavonoids such as quercetin (m/z 302.33 ES+) and kaempferol (m/z 284.26 ES+) detected in positive ionization mode, aligning with their known antioxidant

and anti-inflammatory roles. Phenolic acids included gallic acid (m/z 169.14 ES-), linked to antioxidant activity, and caffeic acid (m/z 180.18 ES+), associated with anticancer effects. Terpenoids like lupeol (m/z 434.48 ES+) and β-sitosterol (m/z 414.58 ES+) were identified, suggesting anti-inflammatory and cholesterol-lowering properties, respectively. Coumarins psoralen (m/z 137.10 ES-) and bergapten (m/z 215.04 ES-), known for photosensitizing and anticancer potential, were also observed. These findings highlight the extract's diverse bioactive potential, which is consistent with the traditional uses of *Ficus* species.

3.2. In-silico skin cancer activity -Docking studies

Gallic acid exhibits superior docking activity compared to other phytochemicals, so gallic acid was used for docking studies. The docking analysis of the 1M17 protein complexed with gallic acid, showing a binding energy of -6.3 kcal/mol, reveals a network of interactions between the ligand and key amino acid residues in the active site. The 3D visualization (**Figure 1A**) highlights the protein's secondary structure, with the ligand nestled within a binding pocket, forming significant interactions. The 2D interaction diagram provides detailed insights into the nature of these molecular contacts. Specifically, gallic acid establishes conventional hydrogen bonds with Asp831, a critical residue stabilizing the ligand through electrostatic interactions.

Additionally, van der Waals interactions are observed with residues such as Leu764, Ile720, Thr766, Glu738, Met742, and Thr830, which contribute to ligand stabilization by enhancing hydrophobic interactions. Furthermore, π-alkyl interactions with Val702, Lys721, and Ala719 suggest an additional stabilizing factor through non-covalent interactions with the ligand's aromatic ring system. The diverse set of interactions, including hydrogen bonding, van der Waals forces, and hydrophobic contacts, indicates that gallic acid has a moderate binding affinity within the protein's active site. The overall binding energy of -6.3 kcal/mol suggests a favourable, yet not extremely strong, interaction, making gallic acid a potential candidate for further optimization in drug design or biochemical studies.

The docking result of the 4QTB protein complexed with the ligand Gallic acid, which has a binding energy of -5.4 kcal/mol, indicates a moderate binding affinity. The molecular docking analysis shows that Gallic acid interacts with key residues in the binding pocket through various non-covalent interactions. The 3D structure (**Figure 1B**) representation highlights the secondary structural elements of the protein, with a surface representation to depict the binding pocket. The 2D interaction map reveals that gallic acid forms conventional hydrogen bonds with residues such as Arg-84 and Ala-52, as indicated by the green dashed lines, which significantly contribute to the stability of the complex. Additionally, the ligand is involved in van der Waals interactions with Asp-184, Gly-186, Glu-88, and Ile-73, which further enhance its binding affinity within the pocket. Pi-alkyl interactions, marked in purple, occur between the benzene ring of Gallic acid and Tyr-53, stabilizing the ligand through hydrophobic interactions. The presence of multiple van der Waals interactions suggests a well-accommodated ligand within the pocket, increasing stability through complementary surface interactions. The hydrogen bonding network between Gallic acid and the protein residues plays a crucial role in the specificity of binding, as hydrogen bonds typically enhance molecular recognition and contribute to binding affinity. Overall, these interactions demonstrate that Gallic acid is well-accommodated in the active site of 4QTB, with a binding energy of -5.4 kcal/mol, indicating moderate stability, suggesting that the ligand-protein interaction is driven by a combination of hydrogen bonding, van der Waals forces, and hydrophobic interactions, which collectively contribute to the ligand's potential as a moderate binder to the protein.

The docking analysis of the 5MP8 protein complexed with gallic acid, which exhibits a binding energy of -5.6 kcal/mol, reveals a range of molecular interactions stabilizing the ligand within the binding pocket. The 3D visualization (**Figure 1C**) on the left side of the image illustrates the protein's secondary structure, highlighting the binding site in a surface representation. The 2D interaction diagram on the right provides a detailed map of the ligand's contacts with surrounding residues. Key interactions include van der Waals forces (green), which contribute to the overall stabilization, and conventional hydrogen bonds (light green) involving residues such as Asn118 and Thr119, which help anchor the ligand through electrostatic interactions. Pi-alkyl interactions (pink) are observed with hydrophobic residues like Leu124, Val162, and Ile164, indicating non-covalent stabilizing effects between the aromatic ring of gallic acid and the protein.

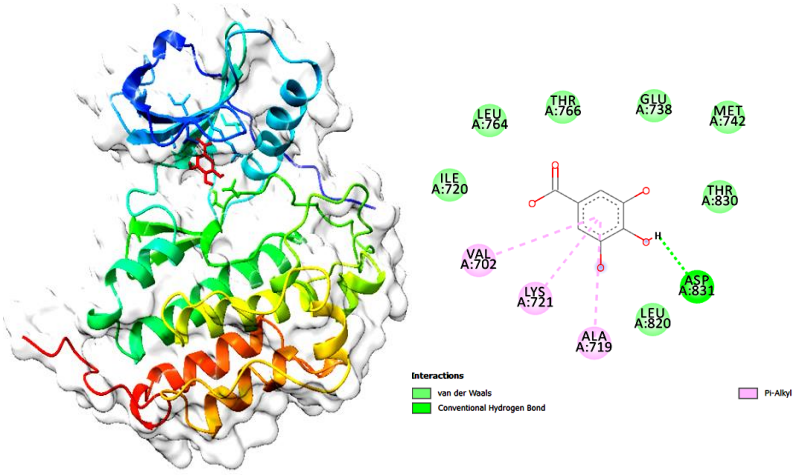

Figure 1A. Molecular docking analysis of the 1M17 protein complexed with gallic acid. The left panel represents the 3D structure of the protein, with a surface representation (white) and a ribbon model colored in a rainbow gradient from the N-terminus (blue) to the C-terminus (red). The ligand, gallic acid, is shown in red within the binding pocket. The right panel depicts a 2D interaction diagram illustrating key molecular interactions between gallic acid and surrounding amino acid residues.

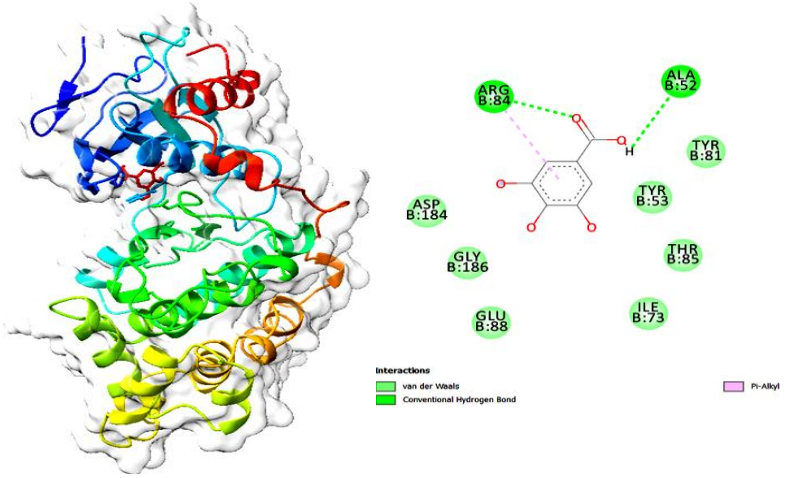

Figure 1B. The docking analysis of the 4QTB protein complexed with Gallic acid, showing key interactions within the binding pocket. The left panel presents the 3D structure of the protein in a ribbon representation with a surface overlay, highlighting the ligand-binding region. The ligand, Gallic acid, is shown in stick representation, interacting with surrounding amino acid residues. The right panel displays the 2D interaction map, which depicts key non-covalent interactions between gallic acid and the protein residues.

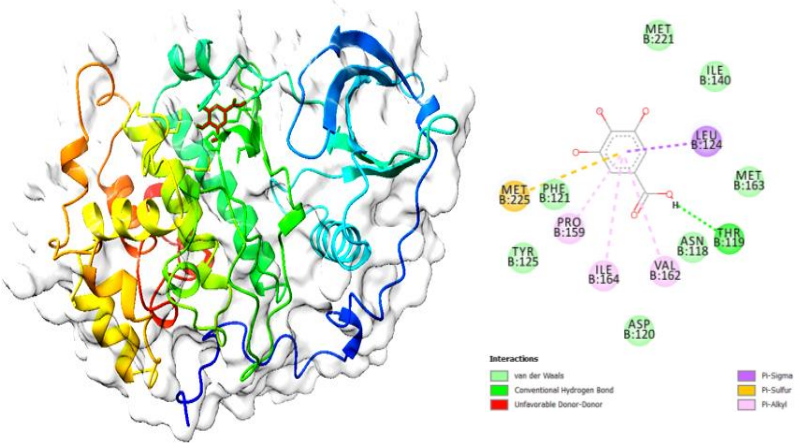

Figure 1C. Molecular docking analysis of 5mp8 protein complexed with gallic acid. The left panel illustrates the 3D structure of the 5MP8 protein, with its secondary structural elements color-coded from blue (N-terminal) to red (C-terminal). The ligand, gallic acid, is shown in stick representation within the binding pocket, surrounded by key interacting residues. The surface representation provides an overview of the protein's binding cavity. The right panel presents a 2D interaction map, depicting specific molecular interactions between gallic acid and the binding site residues.

Additionally, pi-sigma and pi-sulfur interactions (purple and yellow) with residues like Phe121 and Met225 suggest stacking interactions and sulfur-mediated stabilization. The presence of unfavorable donor-donor interactions (red) signifies steric hindrance in specific orientations. This combination of interactions ensures a moderately stable binding of gallic acid to the 5MP8 protein, which could be relevant in functional or inhibitory mechanisms associated with this protein.

3.3. Molecular Dynamics Simulation

Molecular dynamics (MD) simulations were conducted to evaluate the stability and convergence of the 1P7K protein in complex with gallic acid. Over the course of a 200-nanosecond simulation, the complex maintained a stable conformation, as indicated by the root mean square deviation (RMSD) analysis. The Cα-backbone RMSD for 1P7K in the presence of gallic acid remained around 2.0 Å, while the ligand itself showed slightly greater fluctuations (**Figure 2A**). The consistent RMSD values for the protein suggest that the complex reached equilibrium and maintained structural stability throughout the simulation, implying a strong binding affinity between 1P7K and gallic acid. Analysis of root mean square fluctuations (RMSF) revealed only minor fluctuations across most residues, except a noticeable peak at residue 45, where the RMSF exceeded 3 Å; the remainder of the residues exhibited fluctuations below this threshold, indicating a generally rigid protein structure during the simulation (**Figure 2B**). The radius of gyration (Rg), which reflects the compactness of the protein, showed a slight decrease from 20.0 to 19.8 Å (**Figure 2C**), suggesting that the protein adopted a more compact conformation upon ligand binding. Additionally, the number of hydrogen bonds formed between 1P7K and gallic acid remained consistently at two throughout the 200-nanosecond simulation (**Figure 2D**), further supporting the stability and strong interaction within the complex.

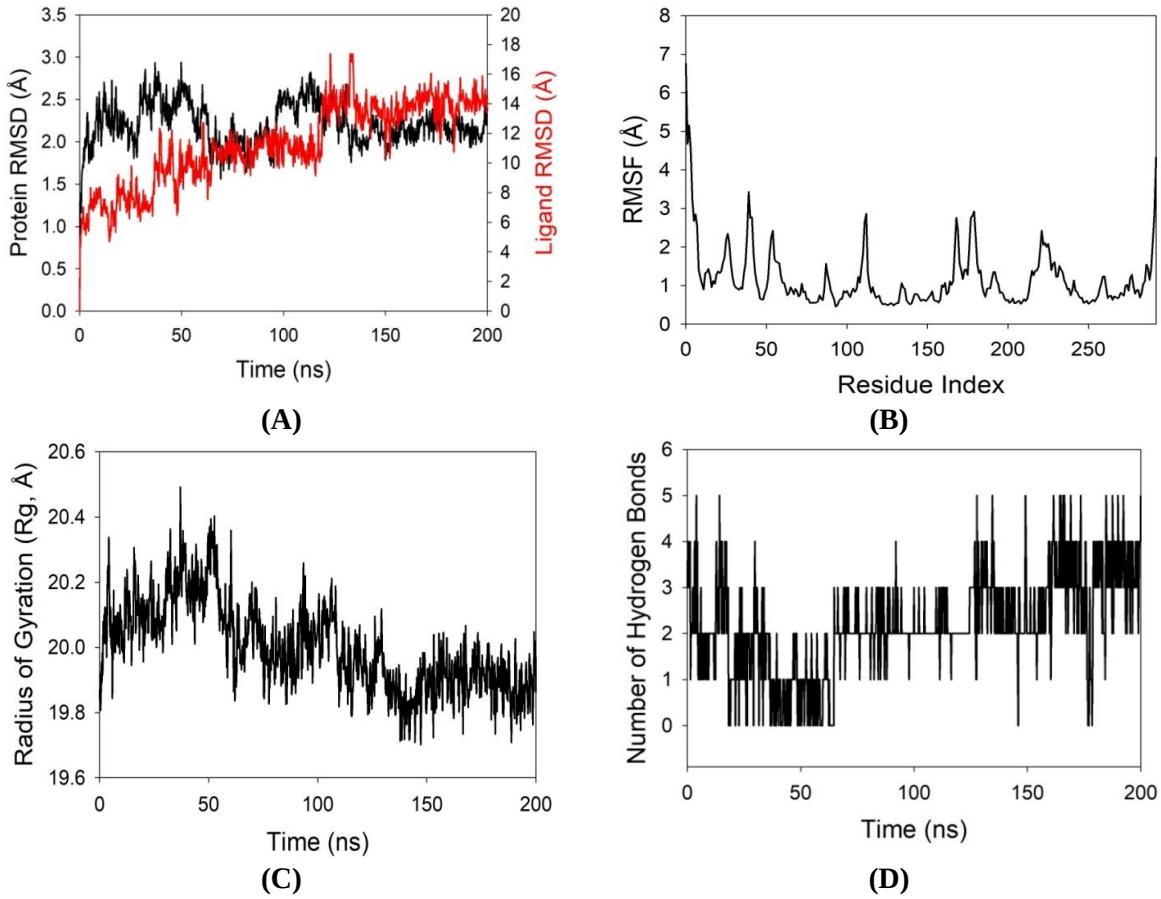

Figure 2. presents the molecular dynamics trajectory analysis over 200 nanoseconds for the 1P7K–gallic acid complex: (A) The RMSD plot displays the stability of the system, with the black line representing the protein and the red line indicating the ligand; (B) The RMSF profile shows fluctuations in the Cα backbone of the protein when bound to gallic acid; (C) The radius of gyration (Rg) plot illustrates changes in the compactness of the protein-ligand complex; and (D) The graph depicts the number of hydrogen bonds formed between the protein and the ligand throughout the simulation.

3.4. Molecular Mechanics Generalized Born Surface Area (MM-GBSA) calculations.

The MM-GBSA binding free energy analysis for the 1P7K–gallic acid complex reveals a favorable interaction, with a total binding free energy (ΔG_{bind}) of –58.61 kcal/mol. This negative value indicates strong binding affinity between gallic acid and the 1P7K protein, consistent with the general reliability of MM-GBSA for estimating protein–ligand binding strengths. Among the energy components, van der Waals interactions (ΔG_{bind} vdW = –23.21 kcal/mol) and lipophilic contributions (ΔG_{bind}Lipo = –15.23 kcal/mol) are significant driving forces for complex formation, while hydrogen bonding (ΔG_{bind}Hbond= –2.99 kcal/mol) and packing interactions (ΔG_{bind}Packing= –7.28 kcal/mol) also contribute favorably. In contrast, the positive values for Coulombic (ΔG_{bind}Coulomb = 26.54 kcal/mol) and solvation (ΔG_{bind}SolvGB = 38.12 kcal/mol) energies reflect the energetic penalties associated with desolvation and electrostatic repulsion, which are common in such calculations. The covalent term (ΔG_{bind}Covalent = 2.22 kcal/mol) makes a minor contribution. Overall, the substantial negative binding energy, primarily driven by van der Waals and hydrophobic effects, suggests that gallic acid binds stably to 1P7K, supporting its potential as a potent ligand for this protein target (**Table 1**).

Table 1. Binding free energy components for the 1P7K bound to GALLIC ACID calculated by MM-GBSA.

Energies (kcal/mol)	1P7K bound to GALLIC ACID
ΔG_{bind}	-58.61
ΔG_{bind}Lipo	-15.23
ΔG_{bind}vdW	-23.21
ΔG_{bind}Coulomb	26.54
$\Delta G_{bind}H_{bond}$	-2.99
ΔG_{bind}SolvGB	38.12
ΔG_{bind}Covalent	2.22
ΔG_{bind}Packing	-7.28

3.5. In-vitro skin cancer activity of the gallic acid

The methanolic extract exhibited significant cytotoxicity against skin cancer cell lines in a clear dose-dependent manner. At the lowest tested concentration (5 µg/ml), cell mortality ranged from 18.46% to 24.16%, while at 10 µg/ml, cytotoxicity increased to 33.63%–39.12%. Further increases in concentration resulted in higher cytotoxic effects, ranging from 50.42% to 55.31% at 15 µg/ml, 69.77% to 76.79% at 20 µg/ml, and a maximum of 80.96% to 88.19% at 25 µg/ml (**Figure 3**). The IC_{50} value, determined from the dose-response curve, was 13.601 ± 0.488 µg/mL, indicating the concentration required to inhibit 50% of the cell population (**Figure 4**).

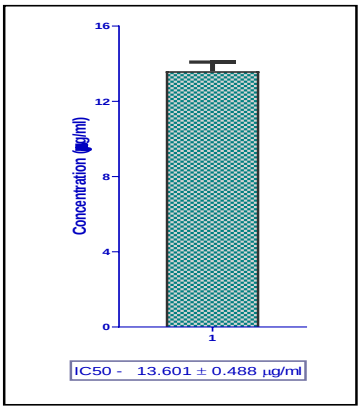

Figure 3. IC_{50} of gallic acid.

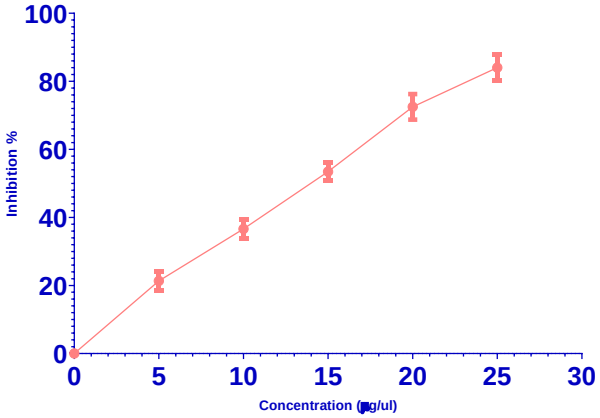

Figure 4. Cell viability assay.

3.6. Apoptotic staining – control &gallic acid.

SK-ML-3 cancer cells were exposed to gallic acid at concentrations of 10 and 20 µg/ml for 24 hours, followed by staining with a combination of acridine orange and ethidium bromide (AO/EB). The cells were then examined using a Zoe Fluorescent Cell Imager (Bio-Rad). Under fluorescence microscopy, viable cells appeared green with normal nuclear morphology. Cells in the early stages of apoptosis displayed yellow fluorescence and showed evidence of chromatin

condensation and nuclear fragmentation. In contrast, late apoptotic cells exhibited orange to red fluorescence, accompanied by pronounced chromatin condensation or fragmentation, resulting in uniformly stained nuclei that were either orange or red (**Figure 5**).

The present study demonstrates that the methanolic extract, particularly gallic acid, exhibits strong cytotoxic effects against skin cancer cell lines in a dose-dependent manner, with an IC50 of 13.601 ± 0.488 µg/ml and a maximal cell mortality of 80.96%–88.19% at 25 µg/ml. These findings are consistent with previous investigations into the anticancer activity of gallic acid. For example, studies on human melanoma (A375.S2) cells highlighted that gallic acid induces significant cell death and apoptosis through multiple mechanisms, including the activation of pro-apoptotic proteins (Bax), upregulation of caspase activity, and downregulation of anti-apoptotic proteins (Bcl-2), resulting in both early and late apoptotic features observed under fluorescence staining closely paralleling the AO/EB staining results [29]. Additional research has reported similar cytotoxic and pro-apoptotic effects of gallic acid in different skin and melanoma cell models, with dose-dependent decreases in cell viability and comparable IC_{50} ranges, further confirming its selective efficacy against cancer cells with limited toxicity toward normal cells [30]. Mechanistically, these studies attribute gallic acid's effect to the increased generation of reactive oxygen species (ROS), disruption of the mitochondrial membrane potential, and both caspase-dependent and -independent apoptotic pathways, all of which are evident in the present cell imaging and apoptotic assessment findings. Collectively, the observed apoptotic patterns, dose-response behavior, and IC_{50} values corroborate existing literature, reinforcing the premise that gallic acid is a potent natural agent for inducing cytotoxicity and apoptosis in skin cancer cells and supporting its potential inclusion in anticancer therapeutic strategies.

4. Conclusion

This study effectively demonstrates the significant anticancer potential of Ficus hispida ethyl acetate extract, with a strong emphasis on gallic acid as a principal bioactive compound. LC-MS analysis identified several key phytochemicals, including quercetin (m/z 302.33), kaempferol (m/z 284.26), and gallic acid (m/z 169.14), all of which are known for their antioxidant and anti-inflammatory properties. In-silico docking studies revealed that gallic acid interacts favorably with multiple skin cancer-related proteins, achieving binding energies of -6.3, -5.6, and -5.4 kcal/mol for 1M17, 5MP8, and 4QTB, respectively. Molecular dynamics simulations confirmed the stability of the gallic acid-protein complexes, with the 1P7K-gallic acid complex showing a low RMSD (2.0 Å), reduced radius of gyration (from 20.0 to 19.8 Å), and stable hydrogen bonding. At the same time, MM-GBSA calculations yielded a strong binding free energy of -58.61 kcal/mol. In vitro assays further validated these findings, as gallic acid exhibited dose-dependent cytotoxicity against skin cancer cells, with an IC50 of 13.601 ± 0.488 µg/mL and an effective induction of apoptosis. These values highlight gallic acid's promise as an effective, plant-derived candidate for future skin cancer therapeutics.

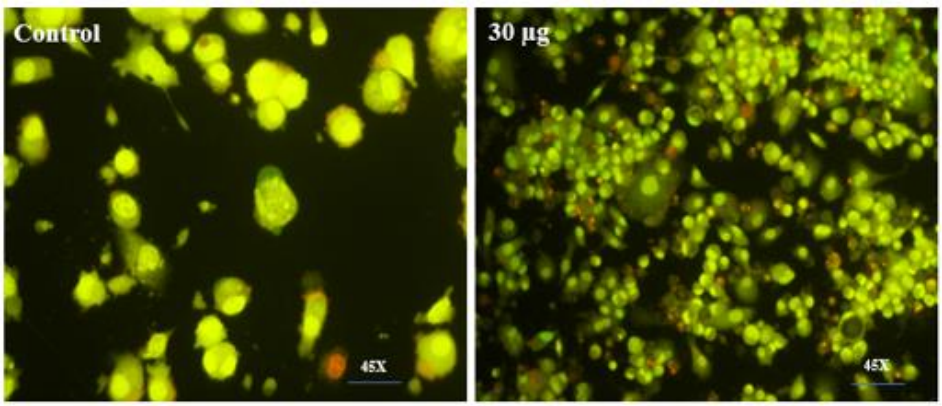

Figure 5. Apoptotic Staining of SK-ME-L-3 Cancer Cells Treated with Control and Gallic Acid (24 h).

Abbreviations

AO/EB: Acridine Orange/Ethidium Bromide
DMEM: Dulbecco's Modified Eagle Medium
DMSO: Dimethyl Sulfoxide
HPLC: High-Performance Liquid Chromatography
IC50: Half-maximal Inhibitory Concentration
LC-MS/MS: Liquid Chromatography-Mass Spectrometry/Mass Spectrometry
LGA: Lamarckian Genetic Algorithm
MD: Molecular Dynamics
MM-GBSA: Molecular Mechanics-Generalized Born Surface Area
MTT: 3-(4,5-dimethylthiazol-2-yl)-2,5-diphenyltetrazolium bromide
NPT: Isothermal–Isobaric Ensemble (constant Number of particles, Pressure, and Temperature)
NVT: Canonical Ensemble (constant Number of particles, Volume, and Temperature)
PBS: Phosphate Buffered Saline
PDA: Photodiode Array (Detector)
RMSD: Root Mean Square Deviation
RMSF: Root Mean Square Fluctuation
Rg: Radius of Gyration
SPC: Simple Point Charge (water model)
VSGB: Variable-dielectric Surface Generalized Born (solvation model)

Acknowledgment

The authors gratefully acknowledge the technical support provided by the Koneru Lakshmaiah Education Foundation, Vaddeswaram, Guntur, Andhra Pradesh. The authors would like to acknowledge the DST for technical support through SR/PURSE/2023/196.

Conflict of interest

The author(s) declared no potential conflicts of interest.

Data availability

Data generated while conducting the research are available to the corresponding author upon reasonable request.

Authors Contributions

Jatla Murali Prakash: Conducted the experimental work, performed data analysis, and Manuscript writing.

Deepti Kolli: Designed the study, supervised the work, manuscript writing and submission.

Authors Orcid numbers:

Jatla Murali Prakash: 0009-0000-5376-6649

Deepti Kolli: 0000-0002-5240-6227

Funding

None.

Using artificial intelligence chatbots

There was no use of artificial intelligence in the making of this article.

References

1. Zhou L, Zhong Y, Han L, Xie Y, Wan M. Global, regional, and national trends in the burden of melanoma and nonmelanoma skin cancer: insights from the global burden of disease study 1990-2021. *Sci Rep*. 2025;15(1):5996. Published 2025 February 18. doi:10.1038/s41598-025-90485-3.
2. Narayanan DL, Saladi RN, Fox JL. Ultraviolet radiation and skin cancer. Int J Dermatol. 2010;49(9):978-986. doi:10.1111/j.1365-4632.2010.04474.x.
3. Leiter U, Eigentler T, Garbe C. Epidemiology of skin cancer. Adv Exp Med Biol. 2014;810:120-140. doi:10.1007/978-1-4939-0437-2_7.
4. Guerra KC, Zafar N, Crane JS. Skin Cancer Prevention. In: StatPearls. Treasure Island (FL): StatPearls Publishing; August 8, 2023.
5. Ng CY, Yen H, Hsiao HY, Su SC. Phytochemicals in Skin Cancer Prevention and Treatment: An Updated Review. Int J Mol Sci. 2018;19(4):941. Published 2018 March 22. doi:10.3390/ijms19040941.
6. Millsop JW, Sivamani RK, Fazel N. Botanical agents for the treatment of nonmelanoma skin cancer. Dermatol Res Pract. 2013;2013:837152. doi:10.1155/2013/837152.
7. Cheng JX, Zhang BD, Zhu WF, et al. Traditional uses, phytochemistry, and pharmacology of Ficus hispida L.f.: A review. J Ethnopharmacol. 2020;248:112204. doi:10.1016/j.jep.2019.112204.
8. Moore RC, Straus E, Dev SI, Parish SM, Sueko S, Eyler LT. Development and Pilot Randomized Control Trial of a Drama Program to Enhance Well-being Among Older Adults. Arts Psychother. 2017;52:1-9. doi:10.1016/j.aip.2016.09.007.
9. Nair S, Meddah B, Aoues A. Melissopalynological Characterization of North Algerian Honeys. Foods. 2013;2(1):83-89. Published 2013 March 7. doi:10.3390/foods2010083.

10. Chu K, Corcoran N, Norden S, Wong LM. New Histopathological & Genetic Features to Improve Active Surveillance Selection for Low-Risk Prostate Cancer. Anticancer Agents Med Chem. 2018;18(7):951-957. doi:10.2174/1871520617666171114105846.
11. Gonzalez-Rey E, Chorny A, O'Valle F, Delgado M. Adrenomedullin protects from experimental arthritis by down-regulating inflammation and Th1 response and inducing regulatory T cells. Am J Pathol. 2007;170(1):263-271.
12. Viaene A, Denys MA, Goessaert AS, et al. Evaluation of the occurrence and diagnose definitions for nocturnal polyuria in spinal cord injured patients during rehabilitation. Eur J Phys Rehabil Med. 2019;55(1):40-46. doi:10.23736/S1973-9087.17.04851-1.
13. Sasidharan S, Chen Y, Saravanan D, Sundram KM, Yoga Latha L. Extraction, isolation and characterization of bioactive compounds from plants' extracts. Afr J Tradit Complement Altern Med. 2011;8(1):1-10.
14. Borges A, José H, Homem V, Simões M. Comparison of Techniques and Solvents on the Antimicrobial and Antioxidant Potential of Extracts from Acacia dealbata and Olea europaea. Antibiotics (Basel). 2020;9(2):48. Published 2020 January 28. doi:10.3390/antibiotics9020048.
15. Abilkassymova A, Aldana-Mejía JA, Katragunta K, et al. Phytochemical Screening Using LC-MS to Study Antioxidant and Toxicity Potential of Methanolic Extracts of Atraphaxis pyrifolia Bunge. Molecules. 2024;29(18):4478. Published 2024 September 20. doi:10.3390/molecules29184478.
16. Morris GM, Huey R, Lindstrom W, et al. AutoDock4 and AutoDockTools4: Automated docking with selective receptor flexibility. J Comput Chem. 2009;30(16):2785-2791. doi:10.1002/jcc.21256.
17. Forli S, Huey R, Pique ME, Sanner MF, Goodsell DS, Olson AJ. Computational protein-ligand docking and virtual drug screening with the AutoDock suite. Nat Protoc. 2016;11(5):905-919. doi:10.1038/nprot.2016.051.
18. Trott O, Olson AJ. AutoDock Vina: improving the speed and accuracy of docking with a new scoring function, efficient optimization, and multithreading. J Comput Chem. 2010;31(2):455-461. doi:10.1002/jcc.21334.
19. Bitencourt-Ferreira G, Pintro VO, de Azevedo WF Jr. Docking with AutoDock4. Methods Mol Biol. 2019;2053:125-148. doi:10.1007/978-1-4939-9752-7_9.
20. Schöller-Gyüre M, Kakuda TN, Witek J, et al. Steady-state pharmacokinetics of etravirine and lopinavir/ritonavir melt extrusion formulation, alone and in combination, in healthy HIV-negative volunteers. J Clin Pharmacol. 2013;53(2):202-210. doi:10.1177/0091270012445205.
21. Jorgensen WL, Maxwell DS, Tirado-Rives J. Development and testing of the OPLS all-atom force field on conformational energetics and properties of organic liquids. J Am Chem Soc. 1996 November 13;118(45):11225-36. doi: 10.1021/ja9621760.
22. Berendsen HJC, Grigera JR, Straatsma TP. The missing term in effective pair potentials. J Phys Chem. 1987;91(24):6269-71. doi: 10.1021/j100308a038.
23. Darden T, York D, Pedersen L. Particle mesh Ewald: An N·log(N) method for Ewald sums in large systems. J Chem Phys. 1993 Jun 15;98(12):10089-92. doi: 10.1063/1.464397.
24. Li J, Abel R, Zhu K, Cao Y, Zhao S, Friesner RA. The VSGB 2.0 model: a next generation energy model for high resolution protein structure modeling. Proteins. 2011;79(10):2794-2812. doi:10.1002/prot.23106.
25. van Meerloo J, Kaspers GJ, Cloos J. Cell sensitivity assays: the MTT assay. Methods Mol Biol. 2011;731:237-245. doi:10.1007/978-1-61779-080-5_20.
26. Plumb JA, Milroy R, Kaye SB. Effects of the pH dependence of 3-(4,5-dimethylthiazol-2-yl)-2,5-diphenyl-tetrazolium bromide-formazan absorption on chemosensitivity determined by a novel tetrazolium-based assay. Cancer Res. 1989;49(16):4435-4440.
27. Liu K, Liu PC, Liu R, Wu X. Dual AO/EB staining to detect apoptosis in osteosarcoma cells compared with flow cytometry. Med Sci Monit Basic Res. 2015;21:15-20. Published 2015 February 9. doi:10.12659/MSMBR.893327.
28. Kasibhatla S, Amarante-Mendes GP, Finucane D, Brunner T, Bossy-Wetzel E, Green DR. Acridine Orange/Ethidium Bromide (AO/EB) Staining to Detect Apoptosis. CSH Protoc. 2006;2006(3):pdb.prot4493.
29. O'Brien MA, Kirby R. Apoptosis: A review of pro-apoptotic and anti-apoptotic pathways and dysregulation in disease. J Vet Emerg Crit Care (San Antonio). 2008;18(6):572-585. doi:10.1111/j.1476-4431.2008.00363.x.
30. Khorsandi K, Kianmehr Z, Hosseinmardi Z, Hosseinzadeh R. Anticancer effect of gallic acid in presence of low level laser irradiation: ROS production and induction of apoptosis and ferroptosis. *Cancer Cell Int*. 2020;20:18.